ACS OMEGA

http://pubs.acs.org/journal/acsodf

Article

Dendrite Growth and Performance of Self-Healing Composite Electrode IPMC Driven by Cu^{2+}

Jiahua Li, Aifen Tian,* Xixi Wang, Zhengxin Zhai, Xinrong Zhang, Bin Feng, Shanshan Yao, and Huiling Du

Cite This: *ACS Omega* 2022, 7, 17575−17582

Read Online

ACCESS | Metrics & More | Article Recommendations | Supporting Information

ABSTRACT: As a kind of flexible intelligent driving material, ionic polymer−metal composite (IPMC) has attracted the attention of researchers due to its advantages of lightweight, large deformation, and fast response. However, the reciprocating bending of IPMC causes cracks to appear on the surface metal electrode layer and reduces the water uptake (WUP). At the same time, the metal particles are extruded, resulting in an increase in resistivity, which affects the driving performance of the materials. Therefore, in this study, considering the preparation cost, Cu-Pt-IPMC using Pt and Cu as a composite electrode with the self-healing system was prepared by electroless plating and Cu^{2+} was used as driving ions that can form a reversible circulation system with a copper electrode. The WUP, surface resistivity, and driving performance were tested and analyzed and the surface roughness was characterized by Matlab. The results show that the dendritic interface electrodes (DIEs) appear at the contact interface between the metal electrode and the film, which extend deeper and wider in the film with the increase in the cycles of autocatalytic platinum plating (ACP-Pt), and the output displacement and blocking force of 61.20 mm and 34.26 mN, respectively, have been achieved in the Cu-Pt-IPMC sample after three cycles of ACP-Pt. Based on these analyses, this study proves that the presence of Cu^{2+} can repair the cracked electrode on the surface of IPMC and reduce the surface electrode resistance, improving the driving performance.

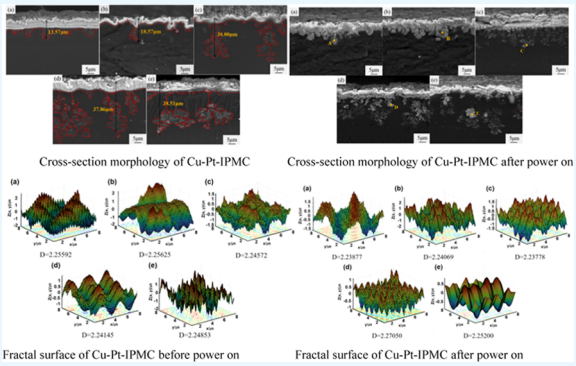

1. INTRODUCTION

Ionic polymer−metal composite (IPMC) is a kind of new intelligent flexible composite material[1−3] with a "sandwich" structure in which the metal is deposited on the surfaces of the ion-exchange membrane as an electrode layer. It is widely used in human medicine, aerospace, bionic engineering, mechanical systems, and other fields.[4−12] The traditional metal electrode materials include Au, Pt, and so on, which have good electrochemical stability and excellent conductivity. However, due to the effect of polarity, surface energy, and preparation process, precious metal electrodes often suffer from serious fatigue, resulting in their falling off.[13] As a result, low-cost metals Cu and Ni, conductive materials such as graphene, multiwalled carbon nanotubes, and a series of polymers are also used as electrode materials.

In 2019, Peng prepared the Cu and Pt composite electrode IPMC (Cu-Pt-IPMC), which achieves greater displacement deflection than the traditional single-electrode IPMC.[14] In addition to the electrode material, the type of working medium (driving ion and solvent) also has an important influence on the stable operation and bending deformation of the IPMC. Different driving ions and solvents have different characteristics and effects on the driving performance of IPMC.[15] In 2018, Wang proposed a new method to prepare a dynamic self-healing electrode using Cu^{2+} as the driving ion. Compared with the traditional IPMC driven by Li^+, the output displacement and force of IPMC driven by Cu^{2+} are 2−3 times higher.[16]

To overcome the problem of surface metal electrode cracking and further explore the performance and driving mechanism of IPMC with a Cu and Pt composite electrode, this study focused on Pt and Cu as the electrode materials to prepare the Cu-Pt-IPMC with a self-healing system driven by Cu^{2+}. By observing its cross-section morphology and dendritic interface electrodes (DIEs),[17] characterizing its surface roughness with Matlab, and testing its water uptake (WUP), surface resistivity, and output performance, the influence of Cu^{2+} as the driving ion on Cu-Pt-IPMC is studied. It has made certain preparations for solving the problems of IPMC surface electrode cracking and easy water loss.

Received: December 28, 2021
Accepted: May 6, 2022
Published: May 19, 2022

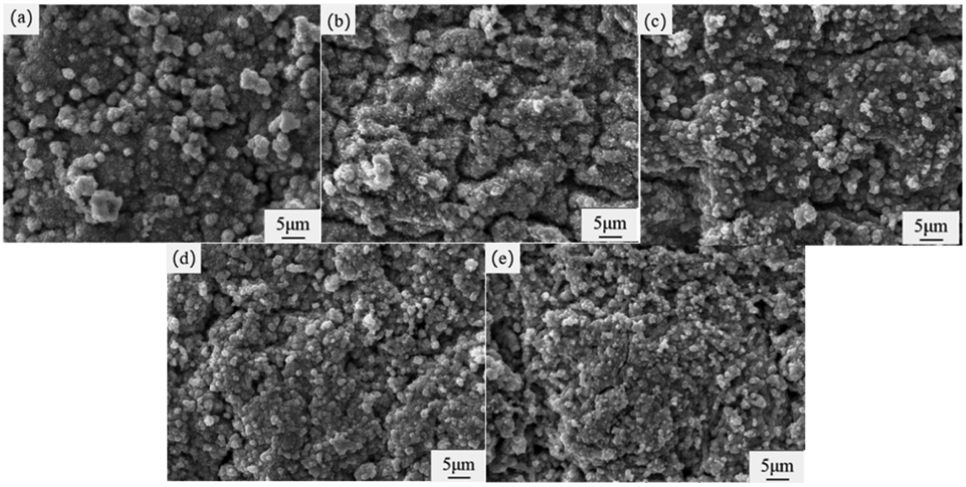

Figure 1. Surface morphology of Cu-Pt-IPMC ((a) 0-Cu-Pt, (b) 1-Cu-Pt, (c) 2-Cu-Pt, (d) 3-Cu-Pt, and (e) 4-Cu-Pt).

2. EXPERIMENTAL SECTION

2.1. Experimental Principle. Under the electric field, when Cu^{2+} is used as the driving ion of Cu-Pt-IPMC, the whole electrochemical reaction is a reversible reaction. The Cu^{2+} on the cathode side of IPMC is reduced to Cu, which fills the electrode cracks and improves the conductivity of the surface electrode. With the progress of the reaction, the copper electrode is consumed after it is generated, forming a self-healing system that repairs cracks and maintains the stability of IPMC. Two electrolytic reactions occur in IPMC when the voltage is applied: copper electrolysis and water electrolysis. The existence of the former reaction weakens the latter and increases the nonaqueous working time of IPMC. After the Cu-Pt-IPMC is powered on, the redox reaction of the anode and cathode is shown in formulas 1 and 2.[14]

Cathodic reaction:

$$Cu^{2+}\cdot 5H_2O + 2e^- \rightarrow Cu + 5H_2O \quad (1)$$

Anodic reaction:

$$Cu + 5H_2O - 2e^- \rightarrow Cu^{2+}\cdot 5H_2O \quad (2)$$

2.2. Preparation Process. In the experiment, Nafion 117 was used as the base film, and Pt and Cu were used as electrode materials to prepare Cu-Pt-IPMC of 30 mm × 10 mm size. The preparation process mainly includes seven processes: pretreatment, ion adsorption ($Pt[(NH_3)_4]Cl_2$ solution), impregnation reduction plating platinum (IRP-Pt), autocatalytic plating platinum (ACP-Pt), ion adsorption ($AgNO_3$ solution), chemical reduction plating copper (CRP-Cu), and ion exchange.

(1) Pretreatment: Both sides of films are ground to a completely opaque state by grid grinding with sandpaper, put in a 2 mol/L hydrochloric acid solution for 20 min, and the temperature is kept constant at 100 °C.

(2) Ion adsorption: The films are put into a 2 mg/mL $Pt[(NH_3)_4]Cl_2$ solution and soaked at room temperature for 12−14 h.

(3) IRP-Pt: The films are put in deionized water and an appropriate amount of $NaBH_4$ is added dropwise. After reacting at different temperatures in a water bath, the samples are soaked in a 0.1 mol/L hydrochloric acid solution for 1−2 h.

(4) ACP-Pt: The films are put into the solution with $Pt[(NH_3)_4]Cl_2$, $NH_3\cdot H_2O$, NH_3OHCl, and $H_2O_4\cdot H_2O$ and circulated several times.

(5) Ion adsorption: The films are put into a 3 g/L $AgNO_3$ solution and kept away from light at room temperature for 12−14 h.

(6) CRP-Cu: 250 mL of deionized water and 6.25 mL of HCHO (37 wt %) are measured, 8.13 g of $C_{10}H_{14}N_2Na_2O_8$, 5.84 g of $C_4H_4O_6K_2$, 5 g of $C_6H_5Na_3O_7\cdot 2H_2O$, 6.67 g of $CuSO_4\cdot 5H_2O$, 0.0042 g of $K_4[Fe(CN)_6]$, and 0.0083 g of $C_{10}H_8N_2$ were placed in the solution and stirred to dissolve. NaOH is added to adjust the pH value between 11 and 12.

(7) Ion exchange: The films are put in the $CuSO_4$ solution with a concentration of 2 mol/L for 1−2 h.

According to the different ACP-Pt cycle times, which is 0, 1, 2, 3, and 4 times, five samples were prepared after the IRP-Pt and CRP-Cu processing, named 0-Cu-Pt, 1-Cu-Pt, 2-Cu-Pt,3-Cu-Pt, and 4-Cu-Pt in this paper.

3. RESULTS AND DISCUSSION

3.1. Characterization and Analysis of Micromorphology. *3.1.1. Surface Morphology.* Figure 1 shows the surface morphology of Cu-Pt-IPMC. It can be seen that the electrode layers deposited on the surface of IPMC are arranged in a granular form. In Figure 1a, the roughened grooves of the Nafion film surface are not completely covered, resulting in narrow and deep holes. In Figure 1b, the electrode surface becomes more dense and fine; however, particle agglomeration begins to occur, leading to the nonuniformity of the electrode layer to a great extent. A large number of Cu particles in Figure 1c−e are agglomerated resulting in an increase in electrode thickness, which is related to the crystal structure and chemical stability of Cu. During electroless plating, the gaps are generated when metal particles nucleate and grow on Nafion film. Then, the reduced metal particles fill the gaps when they are deposited on a Nafion film. However, with the increase in the number of ACP-Pt cycles, due to different growth rates of Cu grains, the reduced metal particles increase and gather together to form aggregates, which become more and more obvious, causing the electrode layer to be no longer dense and uniform.

https://doi.org/10.1021/acsomega.1c07319
ACS Omega 2022, 7, 17575−17582

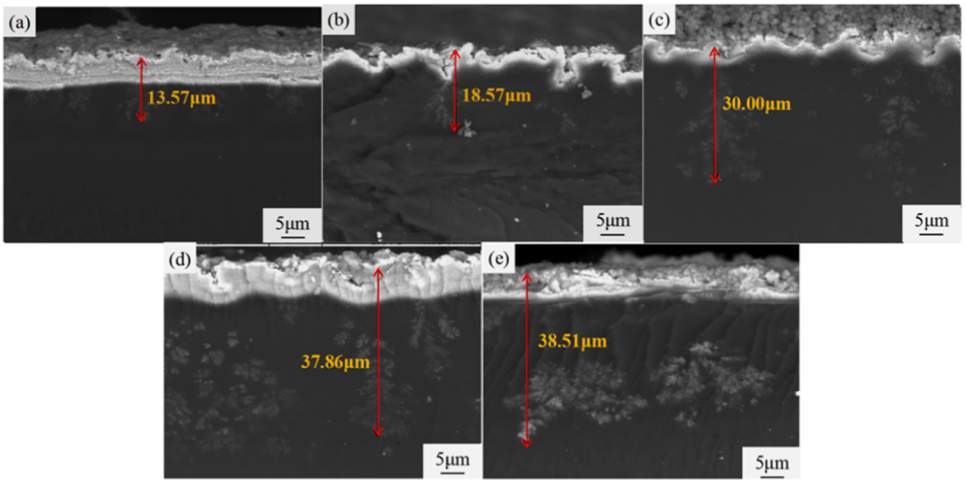

Figure 2. Cross-sectional morphology of Cu-Pt-IPMC ((a) 0-Cu-Pt, (b) 1-Cu-Pt, (c) 2-Cu-Pt, (d) 3-Cu-Pt, and (e) 4-Cu-Pt).

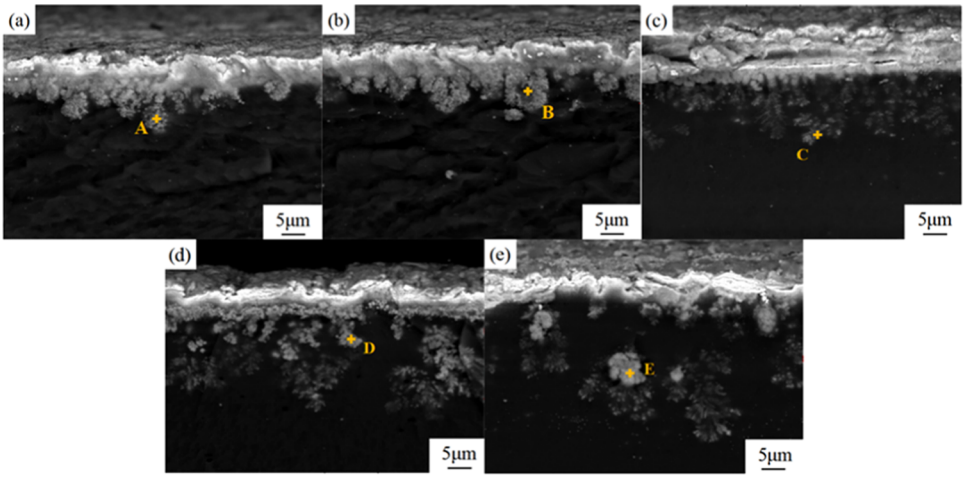

Figure 3. Cross-sectional morphology of Cu-Pt-IPMC after power is on ((a) 0-Cu-Pt, (b) 1-Cu-Pt, (c) 2-Cu-Pt, (d) 3-Cu-Pt, and (e) 4-Cu-Pt).

3.1.2. Cross-Sectional Morphology. Figure 2 shows the cross-sectional morphology of Cu-Pt-IPMC. It can be seen from Figure 2a−e that the coverage of DIEs and the interface area become larger and the electrode layer becomes thicker as the number of ACP-Pt cycles increases. Combined with the coarsening process in the pretreatment process, sandpaper grinding results in the formation of a groove network on the Nafion film, which favors nucleation and contributes to the formation of DIEs. Around the groove, Pt and Cu particles are completely deposited on the film and squeezed together, forming long and continuous DIEs that go deep into the Nafion film. In Figure 2c, the DIEs are composed of a complex branch, which increases the interface area and is conducive to the driving of IPMC. The DIEs in Figure 2d,e obviously become denser and go deeper into the Nafion film, with a penetration depth of up to 38.51 μm.

Figure 3 shows the cross-sectional morphology of Cu-Pt-IPMC after power is on. Compared with Figure 2, Figures 4 and 8 show that a large number of Cu particles accumulate in the interface between the Nafion film and the metal electrode layer after power is on and then extend into the film in the form of droplets (refer to Figure 3a,b). In Figure 3c−e, the branch part of the DIEs obviously changes into thick particles, and the accumulation of particles occurs not only at the interface electrode but also in the Nafion film. Especially in Figure 3e, DIEs extend around the accumulation of a large number of Cu particles, even in the film. As the number of ACP-Pt cycles increases, the DIEs within a Nafion membrane become increasingly obvious, indicating that the electric field may accelerate the emergence of DIEs and improve the driving performance of IPMC.

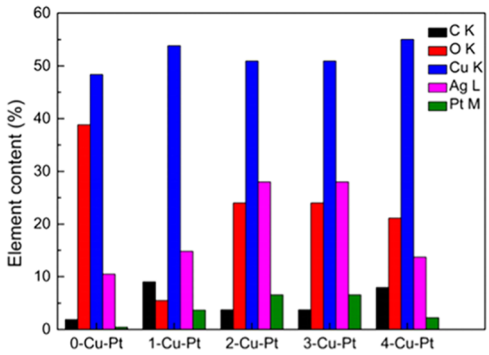

Figure 4. Element content of cross-sectional electrode point scan of Cu-Pt-IPMC.

Figure 4 shows the elemental content of point scanning of the Cu-Pt-IPMC section electrode (points A−E in Figure 3). It can be seen that the content of Cu in the five elements is the

https://doi.org/10.1021/acsomega.1c07319
ACS Omega 2022, 7, 17575−17582

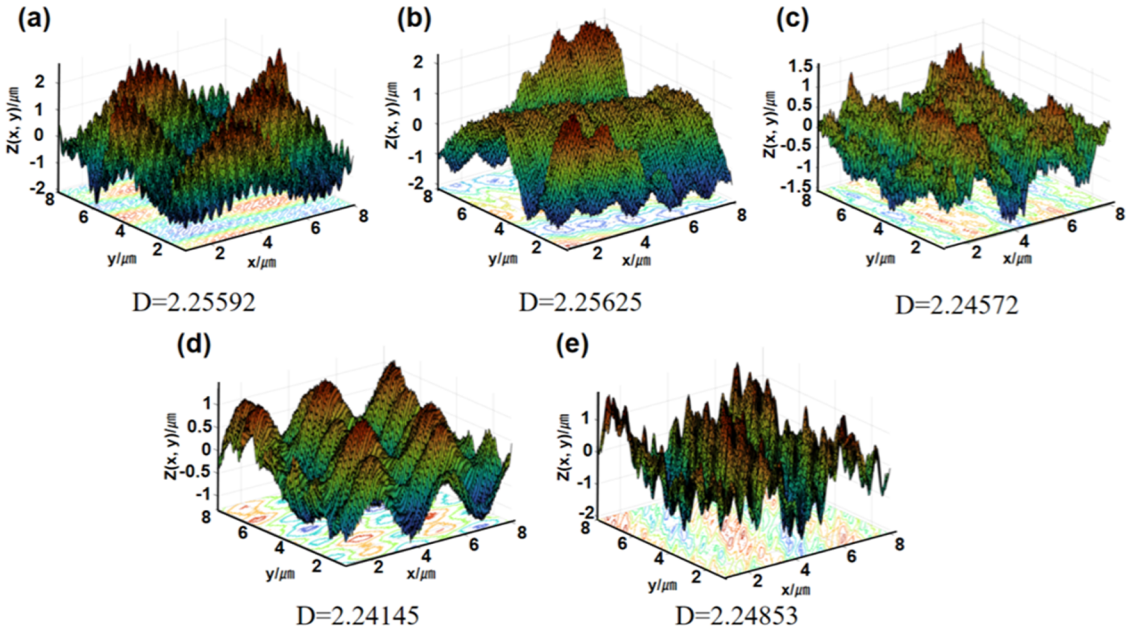

Figure 5. Fractal surface of Cu-Pt-IPMC before power is on ((a) 0-Cu-Pt, (b) 1-Cu-Pt, (c) 2-Cu-Pt, (d) 3-Cu-Pt, and (e) 4-Cu-Pt).

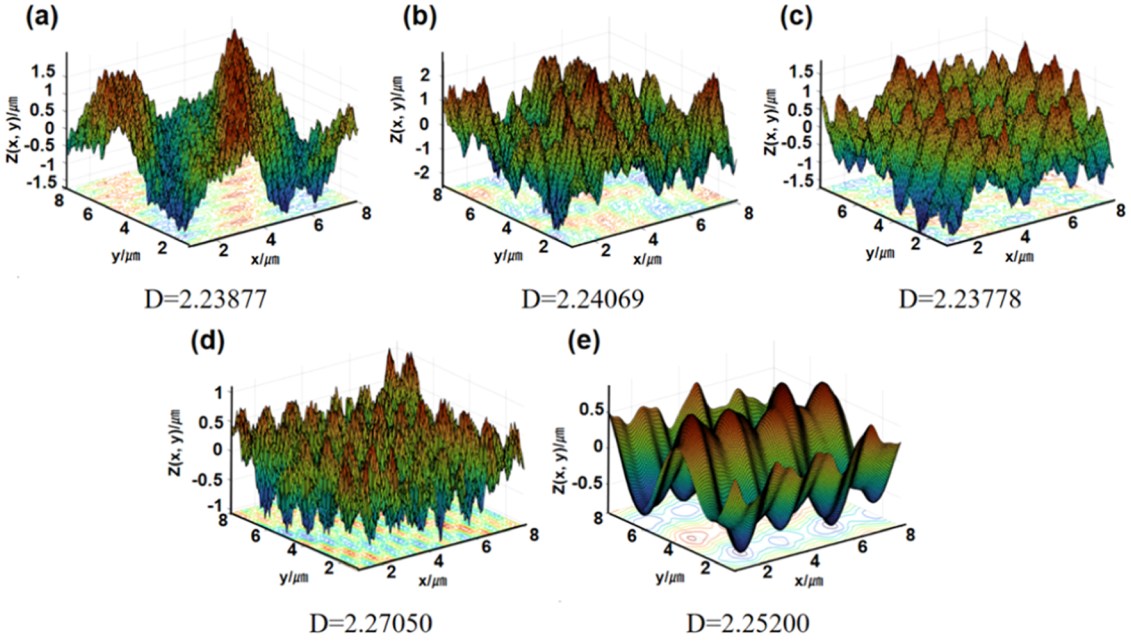

Figure 6. Fractal surface of Cu-Pt-IPMC after power is on ((a) 0-Cu-Pt, (b) 1-Cu-Pt, (c) 2-Cu-Pt, (d) 3-Cu-Pt, and (e) 4-Cu-Pt).

highest. This is because after the IPMC is powered on, Cu^{2+} on the cathode side is reduced to Cu and deposited on the surface of the electrode layer and inside the Nafion film.

3.1.3. Fractal Surface. The interface morphology of IPMC is an irregular and complex state, which can be characterized by fractal theory.[18−23] The larger the fractal dimension is, the more complex the fractal surface morphology is.[24] Figure 5 shows the fractal surface of Cu-Pt-IPMC before power is on, which mainly reflects the roughness of the IPMC surface, and *D* is the fractal dimension. The fractal dimension value of 2.25625 of 1-Cu-Pt is the largest. Combined with Figure 2, it can be seen that the surface of 1-Cu-Pt is also more complex. The reason why the fractal dimension becomes smaller in Figure 5c,d may be that more copper is deposited on the surface of IPMC to fill the cracks during the course of the electroless plating. However, with the increase in the cycles of ACP-Pt up to 4 times, more copper particles are generated at the original crack position due to the growth of DIEs, which leads to the agglomeration of particles and the formation of new gullies. The reason why the fractal dimension of Figure 5e increases again might be that at this time, copper ions are more reduced on the surface of IPMC to form an electric double-layer electrode, which is more flat.

Figure 6 shows the fractal surface of Cu-Pt-IPMC after power is on. It can be seen that the fractal dimension value of 2.2705 of 3-Cu-Pt is the largest. Combined with Figure 6, it can be seen that when the number of cycles of ACP-Pt is 0, 1, and 2, the surface fractal dimension of IPMC after power is on is less than that before power is on, and the opposite situation occurs when the number of cycles is 3 and 4. This may be

https://doi.org/10.1021/acsomega.1c07319
ACS Omega 2022, 7, 17575−17582

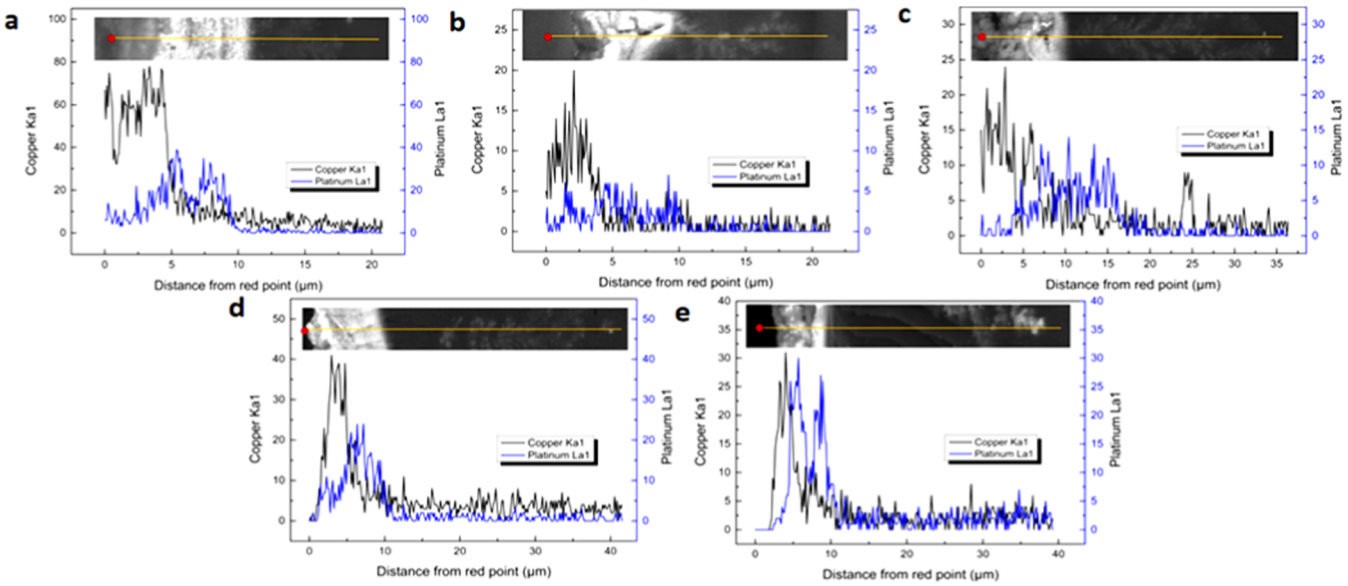

Figure 7. EDS profiles of cross-sectional electrodes of Cu-Pt-IPMC before power is on ((a) 0-Cu-Pt, (b) 1-Cu-Pt, (c) 2-Cu-Pt, (d) 3-Cu-Pt, and (e) 4-Cu-Pt).

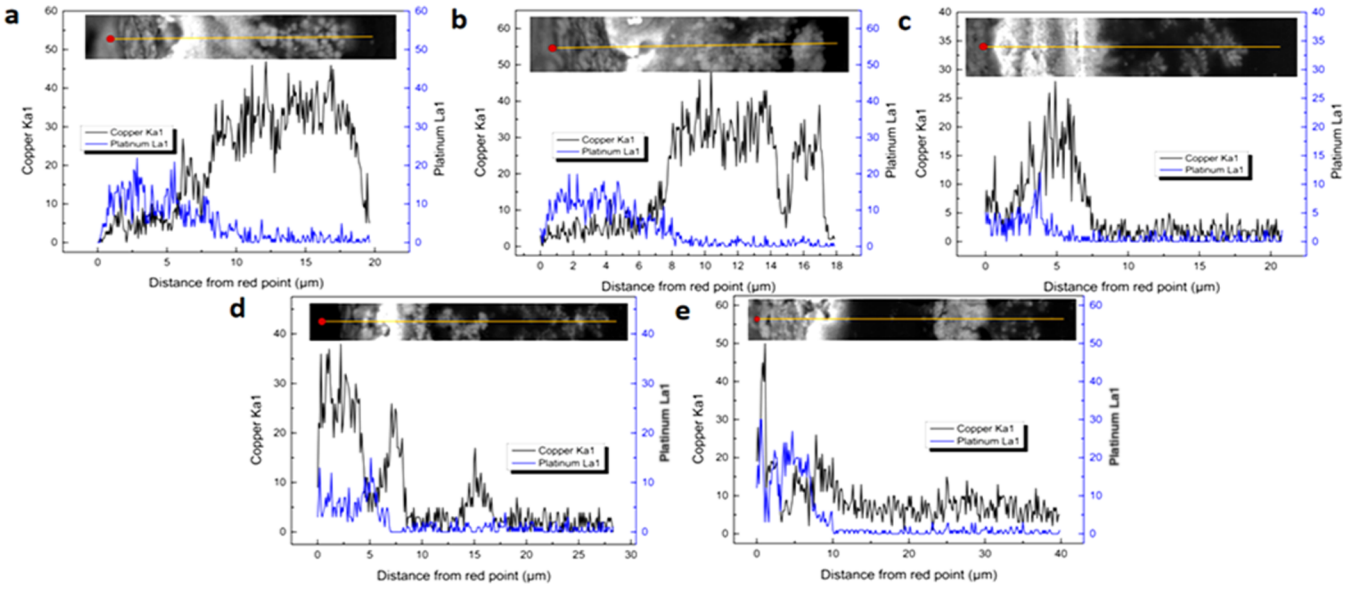

Figure 8. EDS profiles on cross-sectional electrodes of Cu-Pt-IPMC after power is on ((a) 0-Cu-Pt, (b) 1-Cu-Pt, (c) 2-Cu-Pt, (d) 3-Cu-Pt, and (e) 4-Cu-Pt).

because the Cu particles have not yet agglomerated when the number of ACP-Pt is small, and the energization accelerates their agglomeration. It is also possible that the original reduced copper electrode is consumed again due to the power being on, resulting in the rougher surface of IPMC, so the fractal dimension decreases. When the number of ACP-Pt is large, not only does serious agglomeration occur but also more Cu^{2+} on the cathode side becomes copper and is deposited on the electrode surface to fill the cracks. The film surface is smoother and the fractal dimension increases.

3.1.4. Characterization of Cross-Sectional Electrode. To deeply study the DIE structure, we performed EDS. The corresponding EDS profiles are shown in Figure 7. The EDS of the Cu-Pt-IPMC cross-sectional electrode with DIEs before power is on is shown in the figure. The red dot in the figure is on the surface of IPMC, and the end point of the yellow line is inside the Nafion membrane. From the cross-sectional images, we observe that the dendritic distribution displays a perfect DIE structure together with the interfacial electrode of Pt and Cu. As shown in Figure 7a−e, the Cu content is the highest on the electrode surface, but suddenly decreases at the interface and stabilizes inside the Nafion film. The relevant content of Pt is exactly the opposite of Cu when the cycles of ACP-Pt are few, but the same trend occurs for the Pt and Cu content with the increase in the number of ACP-Pt cycles.

Figure 8 shows the EDS of the Cu-Pt-IPMC cross-sectional electrode with DIEs after power is on. Compared with before power is on, the content of Cu in Figure 8a,b increases greatly at the interface and in the film, whereas the content of Pt does not change significantly. Figure 8c,d shows that the Cu content increases significantly at the interface, whereas Figure 8e shows that the copper content decreases at the interface. This is

https://doi.org/10.1021/acsomega.1c07319
ACS Omega 2022, 7, 17575−17582

because Cu^{2+} is reduced to Cu and deposited on the IPMC surface, interface, and gap after power is on, increasing the interface electrode area of IPMC. However, the whole reaction is reversible, as shown in Figure 8e, because the generated copper is consumed by the reaction at the interface of IPMC. This phenomenon can be well explained in combination with Figure 6.

3.2. Water Uptake. The migration of hydrated cation leads to an uneven distribution of ions and water molecules in the Nafion film, resulting in the bending deformation of IPMC. Therefore, the WUP in IPMC has an important influence on the drive performance of IPMC. Figure 9 shows the

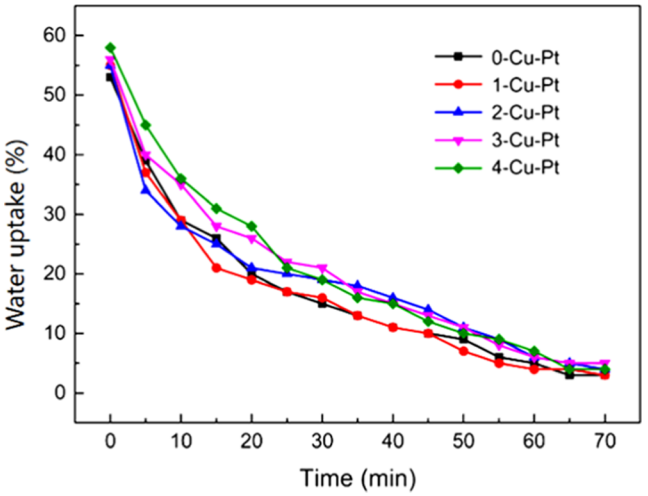

Figure 9. WUP of Cu-Pt-IPMC.

relationship between the WUP of Cu-Pt-IPMC and work time. As shown in the figure, the WUP decreases fastest in the first 5 min with the highest WUP varying in the range of 53−59%, followed by 5−15 min. The WUP decreases slowly in the 15−60 min with the increase in time and remains at about 3−6% after 65 min. Compared with Pt-IPMC under the same test conditions,[25] the WUP of the Cu-Pt-IPMC is 59% and that of Pt-IPMC is 26%, indicating that the cracking phenomenon of the electrode on the IPMC surface is improved.

3.3. Surface Resistivity. The electrode layer on the surface of IPMC plays a conductive role. The resistivity of the electrode has an important impact on the driving performance that the low resistance can promote rapid driving and reduce the response time of IPMC. Figure 10 shows the surface

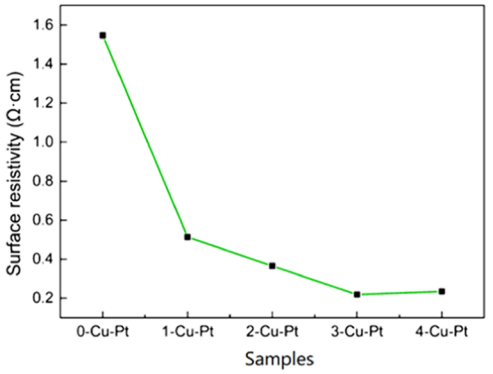

Figure 10. Surface resistivity of Cu-Pt-IPMC.

resistivity of Cu-Pt-IPMC. Among them, the surface resistivities of 0-Cu-Pt and 1-Cu-Pt are quite different, the surface resistivity value of 0.23 Ω·cm of 3-Cu-Pt is the smallest. The deposited metal particles temporarily increase the electrode thickness, compactness, and flatness with the increase in the number of ACP-Pt cycles. However, after a certain number of cycles, the agglomeration of particles causes an uneven distribution of electrode thickness; that is, the compactness and flatness of the surface electrode do not increase but decrease, which has much to do with the fractal surface mentioned above.

3.4. Drive Performance. *3.4.1. Output Displacement.* Figure 11 shows the output displacement of Cu-Pt-IPMC

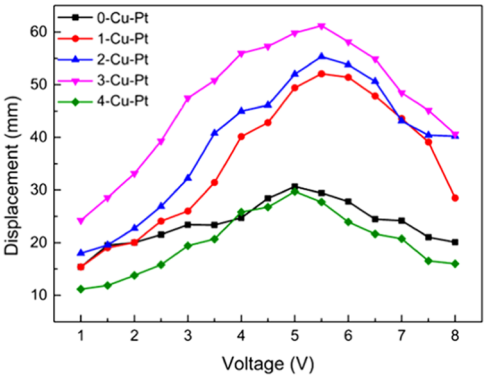

Figure 11. Output displacement of Cu-Pt-IPMC at different DC voltages.

under different DC voltages. As shown in the figure, the output displacement of the IPMC sample first increases and then decreases with the increase in voltage. Among these, 3-Cu-Pt has the maximum output displacement of 61.20 mm at 5.5 V. This is because the number of hydrate cations moving to the cathode increases and the displacement also increases with the increase in voltage. However, when the voltage continues to increase, the water electrolysis reaction is enhanced, and the migration of hydrate cations reaches a saturation state, resulting in no increase in displacement.

3.4.2. Blocking Force. Figure 12 shows the blocking force characteristics of Cu-Pt-IPMC under different DC voltages. As shown in the figure, the blocking force of IPMC increases first and then decreases with the increase of voltage. Among these, 3-Cu-Pt has the maximum blocking force of 34.26 mN at 5 V.

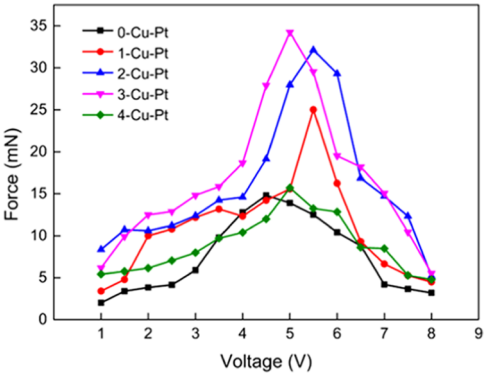

Figure 12. Blocking force characteristics of Cu-Pt-IPMC at different DC voltages.

https://doi.org/10.1021/acsomega.1c07319
ACS Omega 2022, 7, 17575−17582

Combined with the results of output displacement and blocking force, it is concluded that the output characteristics of Cu-Pt-IPMC are not linearly proportional to the cycles of ACP-Pt. The main reason for this is that the thickness and stiffness of the electrode layer on the Nafion film surface become larger with the increase in the number of ACP-Pt cycles. At this time, IPMC is more prone to more cracks and the WUP decreases with the increase in voltage. When the number of hydrate cations in the Nafion film decreases, the expansion and contraction performance becomes weaker. This is the direct reason that the driving performance of IPMC is affected.

3.4.3. Electrochemical Performance of Cu-Pt-IPMC. Figure 13 shows the cyclic voltammetry curve of Cu-Pt-IPMC. The

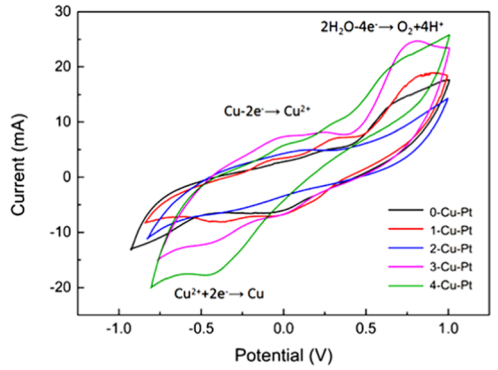

Figure 13. Cyclic voltammogram of Cu-Pt-IPMC.

scanning rate for the experiment is 100 mV/s. As shown in the figure, the voltage range of the sample tested by cyclic voltammetry is −1 to 1 V, there are two peaks in the volt−ampere curve of Cu-Pt-IPMC, which correspond to the redox peak of copper and the electrolysis peak of water,[16] indicating that the oxidation reaction of copper alternates with the reduction reaction of the voltage polarity change. From Figure 13, we observe that there is no redox peak in 0-Cu-Pt and 2-Cu-Pt at −0.5 V; however, there is a reduction peak at −0.1 V for 0-Cu-Pt. At −0.1 V, oxidation peaks appear except for 0-Cu-Pt; between 0.6 and 0.8 V, oxidation peaks also appear in all samples except 2-Cu-Pt. Among them, 4-Cu-Pt has a larger current on the I/E curve, indicating that 4-Cu-Pt has a larger output power. Since the expansion of the metal layer and the reduction reaction of Cu occur on the same side, the formation of copper particles can repair the cracks in the electrode, resulting in the process of dynamic self-healing electrode. It can also weaken the electrolysis of weak water and prolong the working time of IPMC. However, considering the driving performance and the microstructure of the sample, further experiments are needed to analyze the influence of electrochemical performance on the electrical actuation characteristics of IPMC.

4. CONCLUSIONS

In this paper, Cu-Pt-IPMC with a self-healing system was prepared by electroless plating. According to the experimental results, we found the problem of the high cost of IPMC preparation was resolved using copper and platinum as metal electrodes and $CuSO_4$ as an ion-exchange liquid. We also improved the problem that the electrode was easy to crack and led to water loss of IPMC. This manuscript improved the driving performance of IPMC and laid a certain foundation for improving the stable working time and wider adaptability of IPMC.

■ ASSOCIATED CONTENT

Supporting Information

The Supporting Information is available free of charge at https://pubs.acs.org/doi/10.1021/acsomega.1c07319.

Fabrication process flow chart of Cu-Pt-IPMC and schematic diagram of the actual IPMC bending status (PDF)

■ AUTHOR INFORMATION

Corresponding Author

Aifen Tian − *School of Materials Science and Engineering, Xi'an University of Science and Technology, Xi'an 710054, China*; Email: taf@xust.edu.cn

Authors

Jiahua Li − *School of Materials Science and Engineering, Xi'an University of Science and Technology, Xi'an 710054, China*; orcid.org/0000-0003-0170-6112

Xixi Wang − *School of Materials Science and Engineering, Xi'an University of Science and Technology, Xi'an 710054, China*

Zhengxin Zhai − *School of Materials Science and Engineering, Xi'an University of Science and Technology, Xi'an 710054, China*

Xinrong Zhang − *Key Laboratory of Expressway Construction Machinery of Shaanxi Province, Chang'an University, Xi'an 710064, China*

Bin Feng − *School of Mechanical Engineering, Xi'an University of Science and Technology, Xi'an 710054, China*

Shanshan Yao − *Department of Mechanical Engineering, 161 Light Engineering, Stony Brook University, Stony Brook, New York 11794, United States*; orcid.org/0000-0002-2076-162X

Huiling Du − *School of Materials Science and Engineering, Xi'an University of Science and Technology, Xi'an 710054, China*

Complete contact information is available at: https://pubs.acs.org/10.1021/acsomega.1c07319

Notes

The authors declare no competing financial interest.

■ ACKNOWLEDGMENTS

This research was funded by the Key Laboratory Project of Expressway Construction Machinery of Shaanxi Province (300102259510), the Natural Science Foundation of Shaanxi Province (2017JM5042), the SBU-BNL seed grant (1168726-9-63845), the National Science Foundation (NSF) through Award 2129673, the National Natural Science Foundation of China under Grant number (52172099), and Provincial Joint Fund of Shaanxi under Grant number (2021JLM-28).

■ REFERENCES

(1) Chang, M. J.; Cui, W. N.; Liu, J.; Wang, K.; Chai, X. J. Fabrication and photocatalytic properties of flexible g-C_3N_4/SiO_2 composite membrane by electrospinning method. *J. Mater. Sci.: Mater. Electron.* **2018**, *29*, 6771−6778.

(2) Liu, J.; Chang, M. J.; Du, H. L. Fabrication and Photocatalytic Properties of Flexible BiOI/SiO_2 Hybrid Membrane by Electrospinning Method. *J. Nanosci. Nanotechnol.* **2017**, *17*, 3792−3797.
(3) Zhou, W. Y.; Li, T.; Yuan, M. X.; Li, B.; Zhong, S. L.; Li, Z.; Liu, X. R.; Zhou, J. J.; Wang, Y.; Cai, H. W.; Dang, Z. Z. Decoupling of inter-particle polarization and intra-particle polarization in core-shell structured nanocomposites towards improved dielectric performance. *Energy Storage Mater.* **2021**, *42*, 1−11.
(4) Lee, J. W.; Kim, J. H.; Chun, Y. S.; Yoo, Y. T.; Hong, S. M. The performance of Nafion-based IPMC actuators containing polypyrrole/alumina composite fillers. *Macromol. Res.* **2009**, *17*, 1032−1038.
(5) Ma, S. Q.; Zhang, Y. P.; Liang, Y. H.; Ren, L.; Ren, L. Q. High-Performance Ionic-Polymer−Metal Composite: Toward Large-Deformation Fast-Response Artificial Muscles. *Adv. Funct. Mater.* **2020**, *30*, No. 1908508.
(6) Kim, O.; Kim, S. J.; Park, M. J. Low-voltage-driven soft actuators. *Chem. Commun.* **2018**, *54*, 4895−4904.
(7) Nemat-Nasser, S. Micromechanics of actuation of ionic polymer-metal composites. *J. Appl. Phys.* **2002**, *92*, 2899−2915.
(8) Bonomo, C.; Fortuna, L.; Giannone, P.; Graziani, S. A method to characterize the deformation of an IPMC sensing membrane. *Sens. Actuators, A.* **2005**, *123−124*, 146−154.
(9) Yang, L.; Zhang, D. S.; Zhang, X. N.; Tian, A. F. Prediction of the actuation property of Cu ionic polymer metal composites based on backpropagation neural networks. *ACS Omega* **2020**, *5*, 4067−4074.
(10) Gudarzi, M.; Smolinski, P.; Wang, Q. M. Fabrication and transient responses of highly flexible and humidity-insensitive ionic polymer-metal composites in different sensory modes. *J. Intell. Mater. Syst. Struct.* **2019**, *30*, 1653−1666.
(11) Noonan, C.; Tajvidi, M.; Tayeb, A. H.; Shahinpoor, M.; Tabatabaie, S. E. Structure-property relationships in hybrid cellulose nanofibrils/Nafion-based ionic polymer-metal composites. *Materials* **2019**, *12*, No. 1269.
(12) Hui, X.; Tian, A. F.; Wang, Q. Q.; Yang, L.; Zhang, X. R.; Cui, S. S. Research on process optimization of Ag-IPMC. *Integr. Ferroelectr.* **2020**, *210*, 106−115.
(13) Wang, Y.; Chen, H.; Wang, Y.; Zhu, Z.; Li, D. Effect of dehydration on the mechanical and physicochemical properties of gold and palladium-ionomeric polymer-metal composite (IPMC) actuators. *Electrochim. Acta* **2014**, *129*, 450−458.
(14) Peng, W.; Zhang, Y.; Gao, J.; Wang, Y.; Chen, Y.; Zhou, Y. Fabrication and performance of ionic polymer-metal composites for biomimetic applications. *Sens. Actuators, A.* **2019**, *299*, No. 111613.
(15) Shahinpoor, M.; Kim, K. J. Experimental study of ionic polymer-metal composites in various cation forms: actuation behavior. *Sci. Eng. Compos. Mater.* **2002**, *10*, 423−436.
(16) Wang, M.; Yu, M.; Lu, M.; He, Q.; Ji, K.; Liu, L. Effects of Cu^{2+} counter ions on the actuation performance of flexible ionic polymer metal composite actuators. *J. Bionic Eng.* **2018**, *15*, 1047−1056.
(17) Wang, Y. J.; Liu, J. Y.; Zhu, Y. T.; Zhu, D. L.; Chen, H. L. Formation and characterization of dendritic interfacial electrodes inside an ionomer. *ACS Appl. Mater. Interfaces* **2017**, *9*, 30258−30262.
(18) Yang, L.; Zhang, D. S.; Zhang, X. N.; Tian, A. F. Surface profile topography of ionic polymer metal composite based on fractal theory. *Surf. Interfaces* **2021**, *22*, No. 100834.
(19) Deng, K.; Liu, Z.; Deng, J.; Zhao, Y. Variation of surface profile topography based on W-M function model. *Mach. Des. Manuf.* **2017**, *1*, 47−50.
(20) Green, I. Exact spectral moments and differentiability of the Weierstrass-Mandelbrot fractal function. *J. Tribol.* **2019**, *142*, No. 041501.
(21) Mwema, F. M.; Akinlabi, E. T.; Oladijo, O. P.; Fatoba, O. S.; Akinlabi, S. A.; Tlu, S. Advances in manufacturing analysis: fractal theory in modern manufacturing. *Mod. Manuf. Processes* **2020**, 13−39.
(22) Sahoo, P.; Barman, T.; Davim, J. P. *Fractal Analysis in Machining*; Springer: Berlin, Heidelberg, 2011.
(23) Zhang, Y. Y.; Xu, X. Y.; Jin, L. J.; An, Z. L.; Zhang, Y. W. Fractal-based electric field enhancement modeling of vacuum gap electrodes. *IEEE Trans. Dielectr. Electr. Insul.* **2017**, *24*, 1957−1964.
(24) Wu, C. B.; Tian, J.; Liu, C. S.; Chen, Z. H.; Wang, J.; Gong, Y.; Li, L. Y. Evaluation on the methods for calculating the fractal dimension of surface profile curve of coating. *Electroplat. Finish.* **2017**, *036*, 403−408.
(25) Tian, A. F.; Sun, Y.; Wang, X. X.; Li, J. H.; Zhang, X. R.; Wang, H. Y. Effects of Surface Roughening Method on the Performance of Ionic Polymer Metal Composition. *ISAF* **2021**, No. 9477324.

https://doi.org/10.1021/acsomega.1c07319
ACS Omega 2022, 7, 17575−17582